Nonequilibrium Dynamic Phase Diagram for Vortex Lattices

C. J. Olson, C. Reichhardt, and Franco Nori
Department of Physics, The University of Michigan, Ann Arbor, Michigan 48109-1120
(Received 23 April 1998)

The new dynamic phase diagram for driven vortices with varying lattice softness we present here indicates that, at high driving currents, at least *two distinct dynamic phases* of flux flow appear depending on the vortex-vortex interaction strength. When the flux lattice is soft, the vortices flow in independently moving channels with smectic structure. For stiff flux lattices, adjacent channels become locked together, producing crystallinelike order in a coupled channel phase. At the crossover lattice softness between these phases, the system produces a maximum amount of voltage noise. Our results relate spatial order with transport and are in agreement with experiments. [S0031-9007(98)07292-5]

PACS numbers: 74.60.Ge

Nonequilibrium problems involving elastic lattices and disordered media, such as the nature of depinning transitions or the behavior of rapidly driven lattices, appear in a wide variety of systems including superconducting vortex lattices, charge-density waves, and solid-on-solid friction. Much recent interest has been devoted to the motion of a vortex lattice (VL) across a disordered substrate under applied current both at and well beyond depinnng. The reordering of a rapidly driven VL is supported by simulations [1–5] as well as neutron scattering [6] and decoration experiment [7], but the nature of the order that appears remains a subject of debate. In addition, the relationship of the voltage noise observed near depinning to the microscopic vortex motion at higher currents has not been addressed.

Recent work on the behavior of a VL driven by a large current produced conflicting pictures of the VL order, ranging from a crystalline structure [2] to a moving smectic state [8]. In Ref. [9], the VL does not fully recrystallize, but instead enters a moving Bragg glass state with channels. Moreover, Ref. [8] describes the VL in terms of independently moving channels of vortices with overall smectic order. Other theories also focus on channels of vortices [10]. Smectic structure factors [$S(\mathbf{q})$] of the VL were observed in simulations of vortices moving over strong pinning [3,4] in agreement with Ref. [8].

Very recent decoration experiments [11] produced *both* crystallinelike and smectic order of the moving VL, depending on the magnitude of the applied magnetic field. Smectic order appears at low fields, when the vortices interact weakly, and crystallinelike peaks in $S(\mathbf{q})$ appear at high fields, when the vortex interactions are stronger. This suggests that the softness of the VL is important in determining the vortex behavior at high driving currents.

In this paper, we propose a new dynamic phase diagram in which *both* smectic and crystallinelike order appear as the VL softness is varied. Using simulations of current-driven vortices, we clearly define regions of the phase diagram based on $S(\mathbf{q})$, $V(I)$ curves, voltage noise, velocity distributions, direct observation of the lattice, and defect density calculations. We compute experimentally relevant voltage noise spectra [12] at all currents from depinning to high drives, and find evidence for a washboard frequency in the stiff VL as well as broad-band noise in the plastic flow phase. As the VL softens, we observe a novel crossover to a regime in which smectic order is never destroyed even at high drives. At the crossover, the amount of voltage noise generated by the system during depinning is maximum, indicating that experimental voltage measurements can probe the VL order. Our results are in excellent agreement with experiments and have implications for noise measurements in the peak effect regime [13].

We model a transverse two-dimensional slice (in the x-y plane) of a $T = 0$ superconducting infinite slab containing rigid vortices that are parallel to the sample edge ($\mathbf{H} = H\hat{z}$). The vortex-vortex repulsion is correctly represented by a modified Bessel function, $K_1(r/\lambda)$, where λ is the penetration depth. The vortices are driven through a sample with periodic boundary conditions, filled with randomly placed columnar defects, by a uniform Lorentz force $f_d\,\hat{x}$, representing an applied current. The columnar pins are nonoverlapping, short-range parabolic wells of radius $\xi_p = 0.30\lambda$. The maximum pinning force f_p of wells has a Gaussian distribution with a mean value of $f_p = 1.5f_0$ and a standard deviation of $0.1f_0$, where $f_0 = \Phi_0^2/8\pi^2\lambda^3$. The pin density $n_p = 1.0/\lambda^2$ is higher than the vortex density $n_v = 0.7\Phi_0/\lambda^2$. We concentrate on samples $36\lambda \times 36\ \lambda$ in size, containing 864 vortices and 1295 pins. We check for finite size effects using samples that range in size from $18\lambda \times 18\ \lambda$ to $72\lambda \times 72\lambda$ and contain up to 2484 vortices and 3600 pins.

The overdamped equation of vortex motion is $\mathbf{f}_i = \mathbf{f}_i^{vv} + \mathbf{f}_i^{vp} + \mathbf{f}_d = \eta\mathbf{v}_i$, where the total force $\mathbf{f}_i$ on vortex i (due to other vortices $\mathbf{f}_i^{vv}$, pinning sites $\mathbf{f}_i^{vp}$, and the driving current $\mathbf{f}_d$) is given by $\mathbf{f}_i = \sum_{j=1}^{N_v} A_v f_0 \times K_1(|\mathbf{r}_i - \mathbf{r}_j|/\lambda)\mathbf{r}_{ij} + \sum_{k=1}^{N_p}(f_p/\xi_p)\,|\mathbf{r}_i - \mathbf{r}_k^{(p)}|\Theta[(\xi_p - |\mathbf{r}_i - \mathbf{r}_k^{(p)}|)/\lambda]\mathbf{r}_{ik} + \mathbf{f}_d$. Here, Θ is the Heaviside step function, $\mathbf{r}_i$ ($\mathbf{v}_i$) is the location (velocity) of the ith

vortex, $\mathbf{r}_k^{(p)}$ is the location of the kth pining site, ξ_p is the pinning site radius, N_p (N_v) is the number of pinning sites (vortices), $\hat{\mathbf{r}}_{ij} = (\mathbf{r}_i - \mathbf{r}_j)/|\mathbf{r}_i - \mathbf{r}_j|$, $\hat{\mathbf{r}}_{ik} = (\mathbf{r}_i - \mathbf{r}_k^{(p)})/|\mathbf{r}_i - \mathbf{r}_k^{(p)}|$.

Using the monotonic relationship between the shear modulus c_{66} and the dimensionless prefactor A_v of the vortex-vortex interaction term, we model VLs with varying degrees of softness by changing A_v over 3.5 *orders of magnitude*, from $A_v = 0.001$ to $A_v = 6.0$. This is in contrast to previous simulations [3–5,14,15] that considered only an extremely *soft* VL. For each value of A_v, we simulate a voltage-current $V(I)$ curve by initially placing the vortices in a perfect lattice, slowly increasing the driving force f_d from zero to $3.0f_0$ and measuring the resulting voltage signal $V_x = \sum f_x^{(i)}/N_v$.

In order to identify the phase boundaries, each time the driving current f_d increases by $0.08f_0$, we halt the increases in f_d, check that the voltage signal V_x is stationary over time, and then collect detailed velocity and position information for a long time interval, 2×10^5 molecular dynamics (MD) steps, at a single current. For a $36\lambda \times 36\ \lambda$ sample containing 864 vortices, each $V(I)$ curve requires 8×10^6 to 10^7 MD steps to complete, corresponding to about ten days of CPU time on a SPARC Ultra. At each current, we are able to compute accurate voltage noise spectra $S(\omega)$ with a frequency window extending into relatively low frequencies on the order of the vortex time of flight across the sample. We also determine the voltage noise power S_0 in one frequency octave, $S_0 = \int_{\omega_2}^{\omega_1} d\omega\, S(\omega)$, where $S(\omega) = |\int V_x(t) e^{-i2\pi\omega t}\, dt|^2$. The units of frequency are inverse MD time steps. Here, $\omega_0 = 0.027$ and $\omega_1 = 0.054$ were chosen to fall in the middle of our frequency window. The results are not affected if nearby values are used. To measure the order in the VL, we use the Delaunay triangulation of the instantaneous vortex positions to determine the fraction of sixfold coordinated vortices, P_6, and we compute the structure factor, $S(\mathbf{q}) = |\sum_{i=1}^{N_v} e^{i\mathbf{q}\cdot\mathbf{r}_i}|^2/N_v$, of the VL.

The depinning of the VL appears in our simulated $V(I)$ curves, shown in the inset to Fig. 1(a). Since a soft VL is able to deform and take better advantage of the available pinning sites, as A_v decreases the depinning transition shifts to higher driving forces f_d, from $f_d = 0.48f_0$ at $A_v = 6.0$ to $f_d = 1.36f_0$ at $A_v = 0.01$. The depinning also becomes more abrupt for softer VLs, producing a peak in dV/dI that grows in magnitude with lower A_v, as seen in Fig. 1(a). The fact that a *soft VL has a higher depinning current* agrees well with experiments [12,13].

The VL also produces the greatest voltage noise at currents *just above depinning*, when the vortices are in a plastic flow regime. As seen in Fig. 1(b), for each value of A_v the noise power S_0 reaches its peak value $S_{\max}$ at a driving current f_d *above* the current at which the peak in dV/dI occurs. The current f_d at which the peak occurs is independent of the sample size. The spectra $S(\omega)$ near $S_{\max}$ are of the form $S(\omega) \sim 1/\omega$, as illustrated in Fig. 3(A). As A_v decreases and the VL softens, we observe a peak in $S_{\max}$ at $A_v \sim 0.75$, shown in the inset to Fig. 1(b). It is important to point out that this result agrees well with experiments conducted in the peak effect regime [13], in which an observed peak in voltage noise power with changing magnetic field is interpreted to occur due to the softening of the VL as the externally applied magnetic field increases.

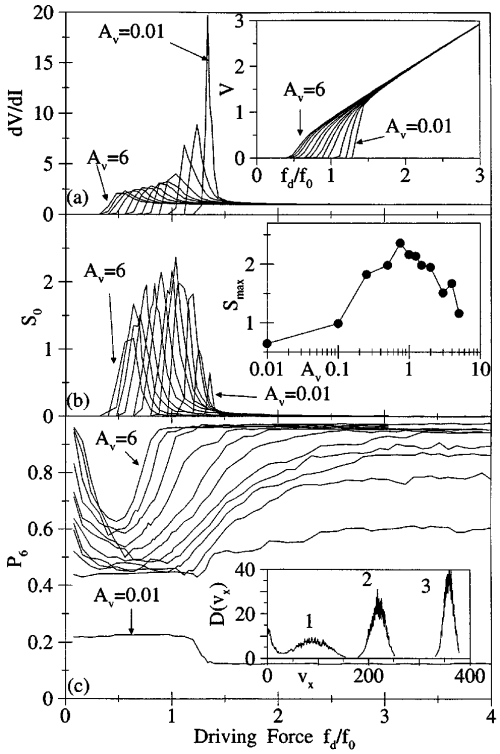

FIG. 1. (a) dV/dI curves for vortex-vortex interactions (right to left) $A_v = 0.01$, 0.1, 0.25, 0.5, 0.75, 1, 1.5, 2, 3, 4, 5, 6. The peak in dV/dI increases in magnitude with decreasing A_v. Inset to (a): Voltage-current $V(I)$ curves for the A_v values listed above. The depinning transition shifts to higher driving currents f_d and becomes more abrupt as A_v decreases. (b) Voltage noise power S_0 versus f_d for the A_v values listed above. In each case the noise power *peaks* during the plastic flow regime. Inset to (b); Maximum noise power $S_{\max}$ as a function of A_v. The peak value of $S_{\max}$ corresponds to $A_v \approx 0.75$, the *same* A_v at which the system crosses between smectic and coupled channel behavior at high drives. (c) Fraction of sixfold coordinated vortices P_6 as a function of f_d for values of A_v listed above. At zero drive and strong VL coupling, $P_6 \sim 1$ since the VL is field cooled. The lowest value of P_6 at each A_v corresponds *exactly* to the peak in dV/dI. The VL eventually reorders to $P_6 \sim 1$ only when $A_v \geq 1$. For $A_v \leq 0.75$, P_6 saturates at a value below 1. Inset to (c): Velocity distribution functions $D(v_x)$ for (1) plastic, (2) smectic, and (3) coupled channel phases.

We quantify changes in the VL structure by calculating the fraction of sixfold coordinated vortices P_6, shown in Fig. 1(c), and the structure factor $S(\mathbf{q})$, shown in Fig. 2. The vortices are initially field cooled, so $P_6 \approx 1$ at

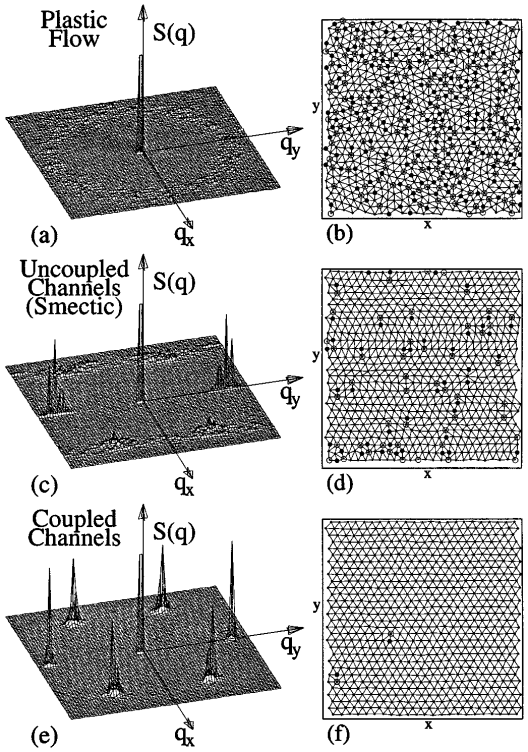

FIG. 2. Structure factor $S(\mathbf{q})$ (a),(c),(e) and Delaunay triangulations (b),(d),(f) of the VL for (a),(b) $A_v = 1.5$, $f_d = 1.12 f_0$ in the plastic flow regime. $S(\mathbf{q})$ is liquidlike, and the VL is filled with defects (marked with circles). (c),(d) $A_v = 0.5$, $f_d = 3.04 f_0$ in the uncoupled channel regime. $S(\mathbf{q})$ has smectic peaks, and the defects in the VL are oriented transverse to the x direction driving force. (e),(f) $A_v = 4$, $f_d = 3.04 f_0$ in the coupled channel regime. $S(\mathbf{q})$ has slightly anisotropic crystallinelike peaks, and the VL contains almost no defects.

$f_d = 0$. At driving currents below the depinning transition, the VL relaxes into the pinning sites, causing a gradual decrease in P_6. The relaxation is most pronounced for soft VLs with low values of A_v. A plastic flow state appears just above depinning, producing a liquidlike structure factor $S(\mathbf{q})$, shown in Fig. 2(a). The Delaunay triangulation in Fig. 2(b) reveals the large number of defects in the VL in this regime. As shown in Fig. 1, we find that the peak in dV/dI corresponds *exactly* to the driving force at which P_6 reaches its *lowest* value. Thus dV/dI can be used to probe the order in the VL.

As seen by the rise of P_6 in Fig. 1(c) for $A_v \geq 0.1$, the VL regains order as the driving force f_d is increased, and the interactions with pinning sites become less important. In stiff VLs with large values of A_v, the defects quickly heal out and P_6 returns to a value near 1 for driving forces f_d not much larger than the pinning force f_p. As A_v is lowered and the VL softens, higher and higher drives f_d must be applied to bring P_6 back to 1. In Fig. 1(c), for $A_v \simeq 0.75$, we see that P_6 saturates at a value less than 1, and does not increase further even after applying driving forces f_d considerably larger than those shown in the figure ($f_d \sim 6 f_0$). The *permanent presence of a significant number of defects* represents an important change caused by the VL softness in the behavior of the system at high driving currents.

Computations of the structure factor $S(\mathbf{q})$, shown in Fig. 2, verify that two different types of VL order appear at high driving currents depending on the lattice softness. When A_v is low and the VL is correspondingly soft, the structure factor $S(\mathbf{q})$ [Fig. 2(c)] has a smectic appearance, with well-defined peaks only along the $q_x = 0$ axis. A Delaunay triangulation of the moving VL, shown in Fig. 2(d), reveals that the vortices are flowing in channels oriented in the x direction (parallel to f_d) and approximately regularly spaced in the y direction (This is in contrast to the plastic flow regime, in which vortices that remain pinned act as barriers and result in vortex motion transverse to the direction of flow, preventing the formation of longitudinal, straight channels.) Vortices in adjacent channels interact so weakly that each channel is able to move independently of nearby channels. All of the defects remaining in the VL have their Burgers vectors aligned *transverse* to f_d, and each channel passes through at least one defect. Thus the channels can easily slip past each other as the defects glide, resulting in an uncoupled channel phase.

If A_v is large and the VL is correspondingly stiff, $S(\mathbf{q})$ has a crystallinelike structure, shown in Fig. 2(e), at high driving currents. The peaks in $S(\mathbf{q})$ are anisotropic, with slightly higher peaks at $q_x = 0$ than at $q_x \neq 0$. For larger samples, the same behavior is observed in $S(\mathbf{q})$, except the peaks are better resolved. The VL is nearly defect-free, as seen in the Delaunay triangulation of Fig. 2(f). The vortices still move in channels oriented in the direction of the drive, but these channels are now locked together by the strong vortex-vortex interactions. Thus, the system is in a coupled channel dynamic state.

We summarize the transitions between different states of the moving VL when A_v and f_d are varied in the phase diagram shown in Fig. 3. The boundary between the pinned and plastic flow phases reflects the increase in the depinning current as A_v decreases, noted earlier. The plastic flow regime, identified by its liquidlike $S(\mathbf{q})$ and by its bimodal vortex velocity distribution [inset to Fig. 1(c)], disappears above $f_d \sim f_p$. For $f_d > f_p$, the softness of the VL determines the behavior of the system. When $A_v \lesssim 0.75$, the structure factor has a smectic appearance for *all* drives $f_d \gtrsim f_p$, corresponding to an *uncoupled* channel (UC) flow regime. For $1 \lesssim A_v \lesssim 3$, the system enters this same smectic UC state immediately after leaving the plastic flow state. At slightly higher driving currents, however, the defect-filled VL enters a transition regime marked by the appearance of weak peaks in $S(\mathbf{q})$ at $q_x \neq 0$. These peaks are significantly smaller than the smectic peaks at $q_x = 0$, but are at least twice as large as the background observed in the smectic phase. Throughout the UC transition regime, the

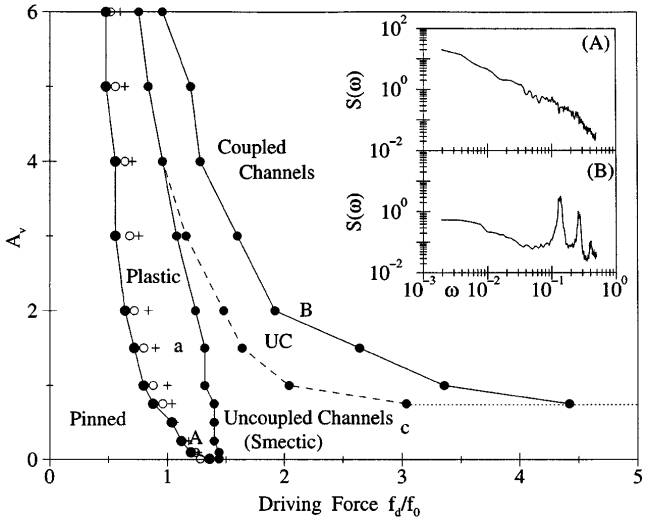

FIG. 3. Dynamic phase diagram for different driving currents f_d and vortex-vortex interaction strengths A_v. At very low drives, the VL is pinned. In the plastic flow phase, we observe *peaks* in dV/dI (crosses) as well as *peaks* in the voltage noise power S_0 (circles). When $A_v \leq 0.75$, the VL flows in uncoupled channels for *all* high driving currents. For larger A_v, the VL passes through a transition region (UC) in which the channels progressively couple, until reaching a reordered state at high drives. A: Typical voltage noise spectrum $S(\omega) \sim 1/\omega$ observed near $S_{\max}$ for $A_v = 0.1$. B: Washboard frequency observed in the coupled channel regime for $A_v = 2$. The magnitude of the narrow band signal decreases in samples larger than the $36\lambda \times 36\ \lambda$ sample shown here. The letters A,B refer to inset plots; a,c, refer to Fig. 2 plots.

channels gradually couple as the number of defects in the VL drops. The unimodal vortex velocity distribution becomes less broad, as in the inset to Fig. 1(c). When $A_v \gtrsim 4$, the system goes directly into this transition state without ever passing through a truly smectic state. Eventually, for all VLs with $A_v \gtrsim 1.0$, the system reaches a *coupled* channel flow phase for large enough values of f_d. The boundary of this phase is identified as the current at which P_6 reaches a value of 1. At the transition $A_v \sim 0.75$ below which the coupled channel phase never appears, the *greatest* maximum noise power $S_{\max}$ is observed, indicating that the noise power could be used as an experimental probe of this transition. At $A_v \sim 0.75$, vortex-vortex and vortex-pin interactions are nearly balanced, allowing the system to sample the largest number of metastable states. The boundaries shown on the phase diagram mark crossover points rather than sharp phase transitions.

In the coupled channel regime, we find a washboard frequency [16] in the voltage noise signal, shown in Fig. 3(B), corresponding to the time required for a vortex to move one lattice constant. The magnitude of this washboard signal decreases when the system size is increased, indicating that the signal appears only when the region of the VL sampled is locked into a single domain. Thus experimentally it would be necessary to probe the voltage over a very small area of a sample to observe a washboard frequency, such as with local Hall probes.

In conclusion, we have obtained a new vortex dynamic phase diagram as a function of lattice softness and driving current. At high driving currents two distinct phases of flux flow appear: in soft lattices, uncoupled channels with a smectic structure, and in stiff lattices, coupled channels with crystallinelike order. A signature of the crossover is observed in the voltage noise, which is largest at the transition between the two phases. In the coupled channel phase, a washboard frequency appears in the voltage noise spectrum for small sample sizes. Our results are in agreement with experiments.

We acknowledge helpful discussions with F. Pardo and S. Bhattacharya, and help from the UM CPC, funded by NSF Grant No. CDA-92-14296. C. O. was supported by NASA.

[1] F. Nori, Science **271**, 1373 (1996); A.-C. Shi and A. J. Berlinsky, Phys. Rev. Lett. **67**, 1926 (1991)
[2] A. E. Koshelev and V. M. Vinokur, Phys. Rev. Lett. **73**, 3580 (1994).
[3] K. Moon *et al.*, Phys. Rev. Lett. **77**, 2778 (1996).
[4] S. Spencer and H. J. Jensen, Phys. Rev. B **55**, 8473 (1997); S. Ryu *et al.*, Phys. Rev. Lett. **77**, 5114 (1996).
[5] M. C. Faleski *et al.*, Phys. Rev. B **54**, 12 427 (1996); C. Reichhardt *et al.*, Phys. Rev. Lett. **78**, 2648 (1997).
[6] U. Yaron *et al.*, Nature (London) **376**, 753 (1995).
[7] A. Duarte *et al.*, Phys. Rev. B **53**, 11 336 (1996); F. Pardo *et al.*, Phys. Rev. Lett. **78**, 4633 (1997); M. Marchevsky *et al.*, *ibid.* **78**, 531 (1997).
[8] L. Balents *et al.*, Phys. Rev. B **57**, 7705 (1998).
[9] T. Giamarchi and P. Le Doussal, Phys. Rev. Lett. **76**, 3408 (1996); Phys. Rev. B **57**, 11 356 (1998).
[10] S. Scheidl and V. M. Vinokur, Phys. Rev. E **57**, 2574 (1998).
[11] F. Pardo *et al.* (to be published).
[12] G. D'Anna *et al.*, Phys. Rev. Lett. **75**, 3521 (1995); T. Tsuboi *et al.*, Phys. Rev. Lett. **80**, 4550 (1998).
[13] A. C. Marley *et al.*, Phys. Rev. Lett. **74**, 3029 (1995).
[14] H. J. Jensen *et al.*, Phys. Rev. B **38**, 9235 (1988).
[15] C. J. Olson *et al.*, Phys. Rev. Lett. **80**, 2197 (1998).
[16] J. M. Harris *et al.*, Phys. Rev. Lett. **74**, 3684 (1995).